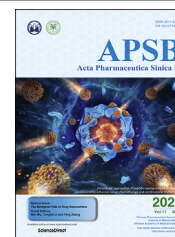




Chinese Pharmaceutical Association  
Institute of Materia Medica, Chinese Academy of Medical Sciences

Acta Pharmaceutica Sinica B

[www.elsevier.com/locate/apsb](http://www.elsevier.com/locate/apsb)  
[www.sciencedirect.com](http://www.sciencedirect.com)



ORIGINAL ARTICLE

# The contribution of absorption of integral nanocrystals to enhancement of oral bioavailability of quercetin



Baode Shen<sup>a,b,†</sup>, Chengying Shen<sup>a,†</sup>, Weifeng Zhu<sup>b,\*</sup>, Hailong Yuan<sup>a,\*</sup>

<sup>a</sup>Department of Pharmacy, Air Force Medical Center, PLA, Beijing 100142, China

<sup>b</sup>Key Lab of Modern Preparation of Traditional Chinese Medicine (TCM), Ministry of Education, Jiangxi University of TCM, Nanchang 330004, China

Received 16 November 2020; received in revised form 27 December 2020; accepted 14 January 2021

## KEYWORDS

Nanocrystals;  
Biological fate;  
Quercetin;  
Pharmacokinetics;  
Biodistribution;  
Oral bioavailability;  
Contribution;  
Drug delivery

**Abstract** In this study, self-discriminating hybrid nanocrystals was utilized to explore the biological fate of quercetin hybrid nanocrystals (QT-HNCs) with diameter around 280 nm (QT-HNCs-280) and 550 nm (QT-HNCs-550) following oral and intravenous administration and the contribution of integral nanocrystals to oral bioavailability enhancement of QT was estimated by comparing the absolute exposure of integral QT-HNCs and total QT in the liver. Results showed that QT-HNCs could reside *in vivo* as intact nanocrystals for as long as 48 h following oral and intravenous administration. A higher accumulation of integral QT-HNCs in liver and lung was observed for both oral and intravenous administration of QT-HNCs. The particle size affects the absorption and biodistribution of integral QT-HNCs and total QT. As compared to QT-HNCs-550, QT-HNCs-280 with smaller particle size is more easily absorbed, but dissolves faster *in vivo*, leading to higher distribution of QT (146.90 vs. 117.91 h·μg/mL) but lower accumulation of integral nanocrystals (6.8 2e10 vs. 15.27e10 h·[p/s]/[μW/cm<sup>2</sup>]) in liver following oral administration. Due to its slower dissolution and enhanced recognition by RES, QT-HNCs-550 with larger diameter shows higher liver distribution for both of QT (1015.80 h·μg/mL) and integral nanocrystals (259.63e10 h·[p/s]/[μW/cm<sup>2</sup>]) than those of QT-HNCs-280 (673.82 & 77.66e10 h·[p/s]/[μW/cm<sup>2</sup>]) following intravenous administration. The absolute exposure of integral QT-HNCs in liver following oral administration of QT-HNCs are 8.78% for QT-HNCs-280 and 5.88% for QT-HNCs-550, while the absolute exposure of total QT for QT-HNCs-280 and QT-HNCs-550 are 21.80% and 11.61%, respectively. Owing to imprecise quantification method, a surprisingly high contribution of integral QT-HNCs to oral bioavailability enhancement of QT (40.27% for QT-HNCs-280 and 50.65% for QT-HNCs-550) was obtained. These results revealed significant difference in absorption and biodistribution between integral

\*Corresponding authors.

E-mail addresses: [zwf0322@126.com](mailto:zwf0322@126.com) (Weifeng Zhu), [yhlpharm@126.com](mailto:yhlpharm@126.com) (Hailong Yuan).

†These authors made equal contributions to this work.

Peer review under responsibility of Chinese Pharmaceutical Association and Institute of Materia Medica, Chinese Academy of Medical Sciences.

<https://doi.org/10.1016/j.apsb.2021.02.015>

2211-3835 © 2021 Chinese Pharmaceutical Association and Institute of Materia Medica, Chinese Academy of Medical Sciences. Production and hosting by Elsevier B.V. This is an open access article under the CC BY-NC-ND license (<http://creativecommons.org/licenses/by-nc-nd/4.0/>).

nanocrystals and overall drugs following oral and intravenous administration of QT-HNCs, and provided a meaningful reference for the contribution of integral nanocrystals to overall bioavailability enhancement.

© 2021 Chinese Pharmaceutical Association and Institute of Materia Medica, Chinese Academy of Medical Sciences. Production and hosting by Elsevier B.V. This is an open access article under the CC BY-NC-ND license (<http://creativecommons.org/licenses/by-nc-nd/4.0/>).

## 1. Introduction

Drug nanocrystals, also known as nanosuspensions, have been drawing growing attention as a useful and successful approach for overcoming the bioavailability limitations of drugs or natural molecules with poor water solubility<sup>1–4</sup>. They are defined as nanosized crystalline particles of pure drug with mean diameter less than 1000 nm, typically 200–500 nm<sup>5,6</sup>. Due to the absence of carrier excipients, drug nanocrystals are considered as carrier-free colloidal dispersion systems with a theoretical drug loading of 100%, typically 50%–90% (w/w)<sup>7–9</sup>. Drug nanocrystals were firstly introduced in the early 1990s and mostly applied to improving the oral bioavailability of poorly soluble drugs because of the enhanced solubility and dissolution<sup>10–13</sup>. During nearly 30 years of evolutionary improvement, drug nanocrystals have been used for various drug delivery systems, *e.g.*, oral, parenteral, transdermal, pulmonary, ocular and targeted drug delivery, etc.<sup>13–18</sup> and different therapeutic applications, such as cancer therapy, inflammatory disease, anti-bacterial actions, anthelmintic treatment, cardiovascular diseases, and so on<sup>2</sup>.

Over the past two decades, the most studies of drug nanocrystals were focused on fabrication methods, formulation optimization, *in vitro* physicochemical evaluation (particle shape, solid state behaviors, solubility and dissolution enhancement, physicochemical stability, etc.), solidification and therapeutic applications, as well as *in vivo* pharmacokinetics and biodistribution based on overall drug analysis<sup>19–23</sup>. The commercial success of tens of nanocrystal products have proven its great potential to delivery hydrophobic drugs<sup>2,9,14</sup>. Nevertheless, limited information about the biological fate of drug nanocrystals is currently known, resulting from the lack of approaches to efficiently and accurately track nanocrystals in biological milieu<sup>24–26</sup>, which limits further development and more commercial success of drug nanocrystals.

With the aim of fully understanding the performance of drug nanocrystals, their intracellular fate or *in vivo* fate have been explored by tracing nanocrystals with autofluorescence<sup>27–30</sup> or tracking fluorescently hybridized nanocrystals<sup>31–37</sup>. The fluorescent hybrid nanocrystals seem to be a promising tool with potential for tracking translocation of nanocrystals in biological environment. Hybrid nanocrystals were developed by the inspiration of dying crystals. Fluorescent molecules are physically integrated inside the lattice of nanocrystals to form hybrid nanocrystals that achieving concurrent disease treatment and bioimaging functionalities<sup>31–35</sup>. However, the conventional fluorescent probes are incapable of discerning nanocrystals *vs.* free probes in the biologic environment, since they also emit fluorescent signals following the dissolution of nanocrystals<sup>25,38,39</sup>.

Recently, environment-responsive fluorescent probes with Förster resonance energy transfer (FRET), aggregation-induced emission (AIE) or aggregation-caused quenching (ACQ) properties have emerged as attractive bioimaging tools for tracing the biological fate of drug nanocrystals and nanocarriers<sup>39–46</sup>. By using the ACQ probes, self-discriminating hybrid nanocrystals were successfully developed to track translocation of drug nanocrystals following oral and intravenous delivery<sup>40–42</sup>. The ACQ probes embedded molecularly inside the lattice of nanocrystals are able to emit strong fluorescence, but form aggregates and quench immediately in the aqueous media following the dissolution of nanocrystals. Therefore, the fluorescence observed represents integral nanocrystals because of completely eliminating free-probe interference. In our previous study, quercetin hybrid nanocrystals (QT-HNCs) were demonstrated to survive the rats' GI tracts for 12–16 h *via* oral administration, and then be integrally absorbed, and accumulated mainly in liver<sup>40</sup>, evidencing long biological life and the absorption of integral nanocrystals *via* oral delivery. Nevertheless, the contribution of absorption of integral nanocrystals to overall bioavailability enhancement is still unknown.

The contribution of absorption of integral nanocrystals to overall bioavailability enhancement is worth exploring, which is of tremendous significance for formulation design and modification of drug nanocrystals with advanced performance both *in vitro* and *in vivo*<sup>17,25</sup>. In previous study, the concentration of integral nanocarriers such as solid lipid nanoparticles or polymeric micelles in lymph or blood can be quantified based on standard curves established by linear regression between fluorescence intensity and nanocarriers concentration<sup>36,47–51</sup>. However, it is unable to be directly quantified integral nanocrystals in biosamples due to its continuous dissolution in aqueous environment. Inspired by the concept of absolute bioavailability, the absolute exposure of integral nanocrystals *in vivo* following oral administration may be estimated by comparing the difference of fluorescence intensity *in vivo* between oral and injection. Then the ratio of the absolute exposure of integral nanocrystals to that of total drug molecules can be regarded as the contribution of absorption of integral nanocrystals to bioavailability enhancement.

In the present study, self-discriminating hybrid nanocrystals were employed to investigate the biological fate of integral QT-HNCs following oral and intravenous administration, and the pharmacokinetics and biodistribution of QT after oral and intravenous administration of QT-HNCs were detected by HPLC method. Then the contribution of absorption of integral QT-HNCs to oral bioavailability enhancement of QT was estimated through dividing the absolute exposure of integral QT-HNCs by that of overall QT.

## 2. Materials and methods

### 2.1. Materials

Quercetin (QT) was purchased from Xi'an Quan'ao Biotech Co., Ltd. (Xi'an, China). Poloxamer 188 (P188) was obtained from Beijing Fengli Jingqiu Pharmaceutical Co., Ltd. (Beijing, China). ACQ probe, P2 ( $\lambda_{\text{abs}}/\lambda_{\text{em}} = 708 \text{ nm}/732 \text{ nm}$ ) was obtained as a gift from the lab of Professor Wei Wu (Fudan University, Shanghai, China). The reference substances of QT and kaempferol (internal standard, IS) were purchased from Chengdu Pufei De Biotech Co., Ltd. (Chengdu, China). Methanol supplied by Fisher Scientific (MA, USA) was of HPLC grade and all other chemical materials were of analytical grade.

Sprague–Dawley (SD) rats (adult male, weighing  $200 \pm 20 \text{ g}$ ) used in the experiments were acquired from SPF (Beijing) Biotechnology Co., Ltd. (Beijing, China) and raised in the laboratory animal room with controlled environment. All animal experiments were conducted following the guidelines on animal welfare approved by the Ethical Committee of Air Force Medical Center, China.

### 2.2. Preparation and characterization of QT-HNCs

QT-HNCs were generated using previously established anti-solvent crystallization method<sup>40</sup> with slight modification. Briefly, 100 mg QT and 20  $\mu\text{g}$  ACQ probe P2 were completely solubilized in 6 mL ethanol (60 °C heating) and then rapidly introduced into 120 mL of aqueous solution containing P188 (0.016%, w/v) that pre-frozen at  $-20 \text{ }^\circ\text{C}$  for 20 min. QT-HNCs with particle size about 550 nm (QT-HNCs-550) and 280 nm (QT-HNCs-280) were obtained by the same precipitation process as our previous report<sup>40</sup> except that an ice water bath instead of water bath at 4 °C.

The particle size and zeta potential of QT-HNCs were analyzed by a Nano-ZS Zetasizer (Malvern, Worcestershire, UK) after appropriate dilution with water. The QT-HNCs were diluted with deionized water and equilibrated for 2 min in the instrument before measurement. For the measurement of fluorescence intensity, 200  $\mu\text{L}$  of QT-HNCs were added into 96-well plates and then determined by a region of interest (ROI) quantification method with IVIS Spectrum Live Imaging System (PerkinElmer, Waltham, MA, USA) at excitation/emission wavelengths of 710/760 nm<sup>40–42</sup>. The fluorescence intensity in this study was presented as total radiant efficiency (TRE) or average radiant efficiency (ARE)<sup>40–42</sup>. The morphological evaluation of QT-HNCs was performed by S-4800 scanning electron microscope (SEM, Hitachi, Tokyo, Japan) at accelerating voltage of 15 kV. After 250 fold dilution with ethanol, an Agilent UV–Visible spectrophotometer (Agilent, Santa Clara, CA, USA) was used to assess QT concentration in QT-HNCs by measuring the absorbance at 375 nm.

### 2.3. Live imaging

Prior to experiment, the abdominal skin of SD rats was shaved and cleaned to eliminate autofluorescence interference of hair and all rats were fasted overnight with free access to water. Rats were randomly divided into two oral groups and two injection groups with three animals in each group. The rats in oral groups were received QT-HNCs with particle size of 280 and 550 nm intragastrically at dose of 90 mg/kg, while QT-HNCs with particle size

of 280 and 550 nm were given to the rats in injection groups by injection *via* caudal vein. Fluorescence images of animals were captured at predetermined time points by the IVIS System under anesthesia with isoflurane.

### 2.4. Pharmacokinetics

After drug administration, about 0.5 mL blood sample was withdrawn at time intervals *via* the orbit vein and then placed into heparinized tube. Fluorescence intensity was immediately determined in 96-well plates based on the ROI method using the IVIS System<sup>40,42</sup>. After fluorescence quantification, the plasma samples were collected by centrifugation using TD-16w centrifuge (BIOBASE, Jinan, China) at 3000 rpm for 10 min at 4 °C and frozen at  $-20 \text{ }^\circ\text{C}$  until analysis.

### 2.5. Biodistribution

To evaluate the biodistribution of QT-HNCs, three rats were sacrificed at each time point post drug administration. After cardiac perfusion with normal saline, the major organs were collected and immediately imaged by the IVIS System. Their fluorescence intensity was quantified by an ROI method<sup>40,42,52,53</sup>. All collected organ samples were frozen at  $-20 \text{ }^\circ\text{C}$  for further analysis.

### 2.6. Analysis of QT in plasma and tissue samples

After being precisely weighed, the isolated organ samples were homogenized with 2 times the volume of normal saline to yield tissue homogenates. A modified acid-hydrolyzed method was employed for the extraction of QT in plasma and tissue homogenates<sup>5</sup>. Briefly, 50  $\mu\text{L}$  kaempferol solution (45.2  $\mu\text{g}/\text{mL}$ , dissolved in methanol) and 200  $\mu\text{L}$  hydrochloric acid (25%, v/v) were added to 200  $\mu\text{L}$  plasma or tissue homogenates and mixed by vortexing vigorously for 90 s and the obtained mixtures were incubated in water-bath at 90 °C for 15 min for enough hydrolyzation. After cooling down, 350  $\mu\text{L}$  of ethanol was added to the hydrolyzates and vortexed for 90 s. Then the supernatant was collected by centrifugation at 8000 rpm for 10 min at 4 °C. The concentration of QT in the supernatant was analyzed on Alltima C18 column (250 mm  $\times$  4.6 mm, 5  $\mu\text{m}$ , Alltech, Guanzhou, China) by Agilent 1200 series HPLC system (Agilent, Santa Clara, CA, USA) with mobile phase of methanol/0.4% phosphoric acid (59:41, v/v) pumped at 1.0 mL/min and detection wavelength at 370 nm and an automatic injection volume of 20  $\mu\text{L}$ .

### 2.7. Data analysis

Pharmacokinetic parameters was obtained by DAS 2.0 Pharmacokinetic software (Boying Corporation, Beijing, China) using statistical moment model. The absolute exposure of integral QT-HNCs was calculated based on the fluorescence intensity in liver according to Eq. (1), while the absolute exposure of total QT was calculated based on the QT content in liver according to Eq. (2). The contribution of integral QT-HNCs in oral absorption was calculated based on the absolute exposure of integral QT-HNCs and total QT in liver according to Eq. (3).

$$\text{Fabs}_{\text{SNCs}}(\%) = \text{AUC}_{0-t(\text{F, oral})} / \text{AUC}_{0-t(\text{F, i.v.})} \times 100 \quad (1)$$

$$\text{Fabs}_{\text{QT}}(\%) = \text{AUC}_{0-t(\text{QT, oral})} / \text{AUC}_{0-t(\text{QT, i.v.})} \times 100 \quad (2)$$

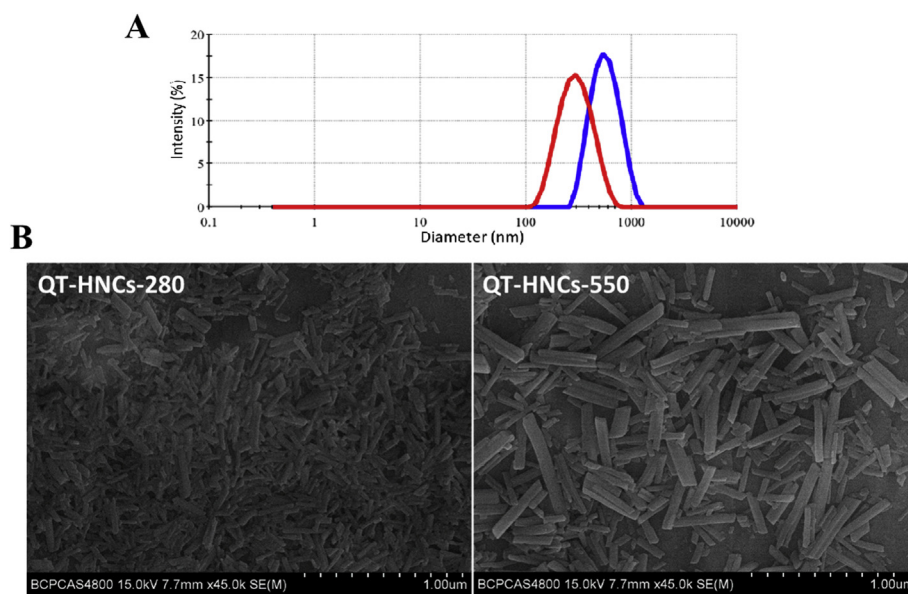


**Figure 1** Particle size distribution (A) and SEM images (B) of QT-HNCs-280 and QT-HNCs-550.

$$\text{Contribution (\%)} = \text{Fabs}_{\text{NCs}} / \text{Fabs}_{\text{QT}} \times 100 \quad (3)$$

where  $\text{Fabs}_{\text{NCs}}$  and  $\text{Fabs}_{\text{QT}}$  represent the absolute exposure of integral QT-HNCs and total QT in liver, respectively.  $\text{AUC}_{0-t}$  (F, oral) or  $\text{AUC}_{0-t}$  (F, i.v.) are the area under the curve to the last measurable fluorescence intensity in liver following oral or intravenous administration of QT-HNCs, while  $\text{AUC}_{0-t}$  (QT, oral) or  $\text{AUC}_{0-t}$  (QT, i.v.) are the area under the curve to the last measurable QT concentration in liver. They were calculated from the fluorescence intensity–time curve or QT concentration–time curve by DAS 2.0 Pharmacokinetic software. Data are expressed as the mean  $\pm$  standard deviation (SD). Difference between two groups was compared by Student's *t*-tests with SPSS 13.0 software (SPSS, Chicago, IL, USA) with  $P < 0.05$  as statistically significant.

### 3. Results and discussion

#### 3.1. Preparation and characterization of QT-HNCs

The established anti-solvent crystallization method was firstly employed for the fabrication of QT-HNCs<sup>40</sup>. The QT-HNCs with particle size around 280 and 550 nm were successfully prepared, but their fluorescence intensity was not desirable. Therefore, a modified anti-solvent crystallization method was used for preparing QT-HNCs in order to achieve higher fluorescent intensity. The P188 aqueous solution was firstly pre-frozen at  $-20\text{ }^{\circ}\text{C}$  for 5, 10, 20 and 30 min and then used as anti-solvent, while an ice water bath was employed to facilitate crystallization during the mixing of the solutions. We found that the fluorescent intensity of QT-HNCs increased significantly with the extension of pre-freezing time of P188 aqueous solution. However, when the P188 aqueous solution was pre-frozen at  $-20\text{ }^{\circ}\text{C}$  for 30 min, the P188 aqueous solution was partially frozen. Therefore, the P188 aqueous solution was pre-frozen at  $-20\text{ }^{\circ}\text{C}$  for 20 min and then was used as an anti-solvent.

QT-HNCs-280 and QT-HNCs-550 produced by the modified anti-solvent crystallization method got average diameter about 280 and 550 nm, respectively, with PDI values less than 0.25 (Fig. 1A and Table 1), indicating a fairly narrow size distribution.

The morphology of QT-HNCs under SEM is appeared to be well-defined rod shape with similar particle size to the results from particle size analysis (Fig. 1B). The zeta potential and QT content of QT-HNCs are  $-20\text{ mV}$  and  $18\text{ mg/mL}$ , respectively. All these abovementioned physicochemical properties are the same as the results of our previous study<sup>40</sup>. Differently, the fluorescence intensity of QT-HNCs is higher than that of our previous report, which may be attributed to higher difference of temperature during the anti-solvent precipitation process. The temperature of solvent influences the solubility of QT, and therefore temperature variation was adopted to facilitate rapid crystallization, contributing to embedding more P2 probes into the lattice of QT-HNCs and thus leading to higher fluorescence intensity of QT-HNCs.

#### 3.2. Live imaging

The live images and fluorescence quantification following oral and intravenous administration of QT-HNCs are shown in Fig. 2 and Supporting Information Fig. S1. No P2 quenched solution was set as control group, because the P2 quenched solution has been reported to be produced no fluorescence interference following oral and intravenous administration<sup>40–42</sup>. Oral administration of QT-HNCs exhibits significant fluorescence signals in the abdomen region of rats (Fig. 2A), which is in agreement with our previous study<sup>40</sup>. The fluorescence intensifies gradually in the first 2 h, then declines and finally vanishes (Fig. S1A). This phenomenon can be considered as a result of the initially intragastric dispersion of QT-HNCs post administration, and afterwards transportation and dissolution of QT-HNCs *in vivo*<sup>40,41</sup>. The fluorescent signals in the abdomen region of rats are still observed at 12 h for QT-HNCs-280 and 24 h for QT-HNCs-550, indicating a long biological life of QT-HNCs *in vivo*, which is probably attributed to their slow dissolution due to limited amounts of dissolution media in the GI tract<sup>54</sup>. QT-HNCs-280 group shows shorter retention time and slightly weaker fluorescence *in vivo* as compared to QT-HNCs-550, which may be ascribed to its faster dissolution owing to the smaller particle size<sup>55,56</sup>.

Following intravenous administration, both of QT-HNCs-280 and QT-HNCs-550 are pervasively distributed throughout the

**Table 1** Physicochemical properties of QT-HNCs-280 and QT-HNCs-550.

Formulation	Particle size (nm)	PDI	Zeta potential (mV)	TRE [p/s]/[ $\mu\text{W}/\text{cm}^2$ ] $\times 10^9$	QT content (mg/mL)
QT-HNCs-280	272 $\pm$ 12	0.18 $\pm$ 0.02	-20.6 $\pm$ 2.1	10.8 $\pm$ 0.05	18.37 $\pm$ 0.33
QT-HNCs-550	538 $\pm$ 18	0.22 $\pm$ 0.04	-22.1 $\pm$ 3.3	9.5 $\pm$ 0.06	18.10 $\pm$ 0.24

Data are expressed as the mean  $\pm$  SD ( $n = 3$ ).

body until 48 h (Fig. 2B and Supporting Information Fig. S2B), indicating long-circulating capability and slow dissolution of QT-HNCs *in vivo*. The long circulating time of QT-HNCs *in vivo* may be due to the camouflage effect of P188 absorbed on the surfaces of nanocrystals<sup>57</sup>. Additionally, more significant fluorescent signals are observed in the abdominal area (RES organs) of rats than its surrounding area. QT-HNCs-550 group shows stronger fluorescence in the abdominal area and longer retention time than those of QT-HNCs-280. These results imply that QT-HNCs may accumulate in RES organs following intravenous administration and the QT-HNCs with larger diameter accumulate in more amount. Similar distribution feature were also observed in previous report with intravenous administration of curcumin hybrid nanocrystals<sup>42</sup>.

### 3.3. Pharmacokinetics of integral QT-HNCs

The fluorescence of the blood following intravenous administration of QT-HNCs was recorded by the IVIS system (Fig. S2) and quantified by an ROI method based on ARE (Fig. 3). Although without significant difference, QT-HNCs-280 group shows slightly higher ARE values than that of QT-HNCs-550 group, which may be because more amount of QT-HNCs-550 are captured by RES organs as proposed in live imaging study and confirmed by *ex vivo* imaging of organs (Fig. 4). Only 25% fluorescence remained in blood at 4 h for both of QT-HNCs-280 and QT-HNCs-550 as compared to fluorescence measured at 5 min, while there is about 8% fluorescence still left at 24 h for QT-HNCs-280, and 4% left at 48 h for QT-HNCs-550. The results demonstrate that QT-HNCs can be fast cleared from circulation following intravenous administration, but remain certain long-circulating capability, further proving the long-circulating effect of QT-HNCs *in vivo*. No fluorescent signal can be found in blood after oral administration of QT-HNCs (Fig. S2), implying relatively low levels of integral QT-HNCs in circulation.

### 3.4. Biodistribution of integral QT-HNCs

The biodistribution of integral QT-HNCs following oral and intravenous administration of QT-HNCs was investigated by fluorescence imaging of each organ. Fig. 4 shows *ex vivo* images of major organs following oral and intravenous administration of QT-HNCs, respectively. The oral absorption of integral QT-HNCs is directly evidenced by the observed fluorescence in different organs following oral administration of QT-HNCs. In spite of no fluorescence in blood, we observed obvious fluorescent signals in liver and lung with retained time more than 48 h, for both of QT-HNCs-280 and QT-HNCs-550, after oral administration (Fig. 4A). Additionally, a faint fluorescence was also found in spleen from 8 to 12 h. It should be noted that the weak fluorescent signal found in kidney at each time point can be considered as negative interference, because the kidneys of the blank rats also exhibited weak fluorescent signals. Moreover, the biodistribution of integral QT-HNCs is significantly influenced by particle size. The fluorescence in liver peaks at 8 h for QT-HNCs-280, while 12 h for QT-HNCs-550, indicating faster absorption of QT-HNCs with the smaller particle size, which complies with previous finding that smaller nanoparticles can be absorbed more quickly *via* the intestinal epithelium<sup>58</sup>. QT-HNCs-280 group shows weaker fluorescence in liver than that of QT-HNCs-550 group. The same reason that QT-HNCs with the smaller particle size dissolves faster can be employed to interpret this phenomenon<sup>55,56</sup>.

As shown in Fig. 4B, the fluorescent signals appears in all organs as early as 5 min and remains for at least 48 h following intravenous administration of QT-HNCs, with strongest fluorescence in liver, followed by lung, demonstrating high accumulation of integral QT-HNCs in organs of the reticuloendothelial system (RES). A relatively high accumulation of integral QT-HNCs in RES organs (liver and lung) can be found following oral or intravenous administration of QT-HNCs (Fig. 4). An acceptable explanation is that nanoparticles reaching the systemic circulation may follow similar fate, which are generally recognized,

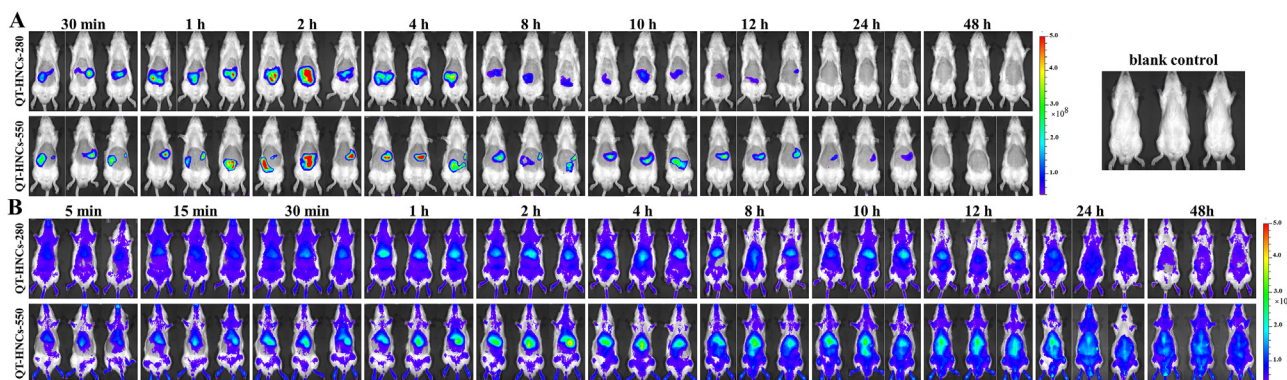


**Figure 2** *In vivo* live imaging of SD rats following oral (A) and intravenous (B) administration of QT-HNCs-280 and QT-HNCs-550, respectively. The rats treated without of QT-HNCs were used as blank control.

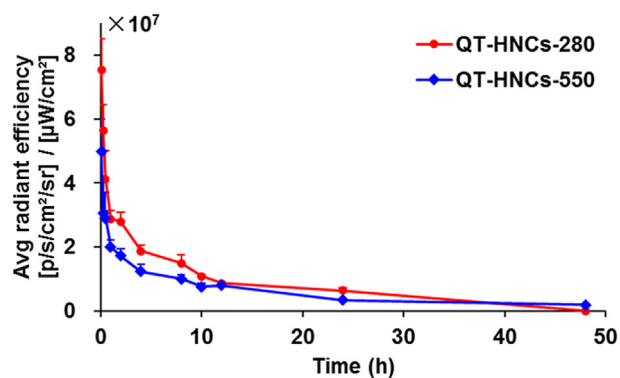


**Figure 3** Fluorescence quantification of blood following intravenous administration of QT-HNCs-280 and QT-HNCs-550. Data are presented as mean  $\pm$  SD ( $n = 3$ ).

opsonized and ultimately captured by macrophages residing in RES organs<sup>42,59</sup>. Similar to oral administration, the fluorescence of liver peaks at 15–30 min for QT-HNCs-280, while about 1–2 h for QT-HNCs-550. An obvious stronger fluorescence in liver can be observed in QT-HNCs-550 group as compared to QT-HNCs-280 group. This can be explained by the reasons that smaller nanocrystals may achieve a faster uptake by hepatocyte, resulting in rapidly peaking, but they dissolve faster due to its smaller particle size, leading to less fluorescence retention in liver.

The fluorescence quantification of major organs based on TRE and ARE is displayed in Fig. 5 and Supporting Information Fig. S3. The TRE values of liver and lung follow a pattern of gradual increment in first and decrement afterwards following oral administration of QT-HNCs (Fig. 5A and B). Similar results can be obtained from the ARE values (Figs. S3A and S3B). After intravenous administration of QT-HNCs, the TRE values in various organs shows an order of liver > lung > spleen  $\approx$  heart  $\approx$  kidney, while the ARE values in various organs is in an order of lung > liver > spleen > heart > kidney (Fig. 5C and D). Both of liver and lung show much higher TRE and ARE values than those of other organs, confirming high accumulation of integral QT-HNCs in RES organs. The ARE and TRE values of liver and lung present in reverse order, which is probably due to their different analysis method. The ARE values are obtained by dividing the TRE values

by the total area of organ. The area of the lungs is smaller than that of the livers, therefore, leading to higher ARE in lungs.

In order to estimate the total amounts of integral QT-HNCs in various organs, the  $AUC_{0-t}$  of fluorescence intensity was obtained from the TRE and ARE profiles by Pharmacokinetic software DAS 2.0 using statistical moment model (Table 2 and Supporting Information Table S1). For oral administration of QT-HNCs-550, the  $AUC_{0-t}$  of the lungs was not obtained, because that the DAS 2.0 could not perform data fitting and calculate the  $AUC_{0-t}$  due to its fewer data points. Following oral and intravenous administration of QT-HNCs, QT-HNCs-550 group shows significantly higher  $AUC_{0-t}$  in tested organs than that of QT-HNCs-280 group (Table 2 and Table S1). This can be explained by slower dissolution of QT-HNCs with larger particle size and enhanced recognition by RES<sup>42,55,56</sup>. Both of TRE and ARE, QT-HNCs-280 and QT-HNCs-550 show higher  $AUC_{0-t}$  in liver and lung than that in other organs following oral and intravenous administration, further confirming high accumulation of integral QT-HNCs in RES organs.

### 3.5. Drug pharmacokinetics and biodistribution

QT was reported to circulate in plasma in conjugated forms such as glucuronides and sulfates<sup>60</sup>. To clear all ester-bonds of QT conjugates, a modified acid-hydrolyzed method was therefore adopted to extract QT from plasma and tissue homogenates<sup>5</sup>. The QT concentrations in plasma and tissue homogenates were determined by HPLC with kaempferol as an internal standard. The regression equations of QT in plasma and tissue homogenates were established by taking QT concentration as the abscissa and the peak area ratio ( $Y$ ) of QT to kaempferol as the ordinate. A good linear relationship between  $Y$  and QT concentration can be observed within the specific concentration range for plasma and tissue homogenates (Supporting Information Table S2). The mean recovery of QT in plasma and tissue homogenates is 86.42%–97.93%, with RSD less than 8%. The intra- and inter-day precisions are less than 7%.

The mean plasma QT concentration *versus* time curves after oral and intravenous administration of QT-HNCs are listed in Fig. 6 and the main pharmacokinetic parameters are shown in Table 3. As compared to QT-HNCs-550, a higher plasma QT concentrations was determined in most time point following oral administration of QT-HNCs-280. Moreover, QT-HNCs-280 gets significant higher  $AUC_{0-t}$  of 82.40 h  $\cdot$   $\mu$ g/mL and  $C_{max}$  of 3.70  $\mu$ g/mL than those of

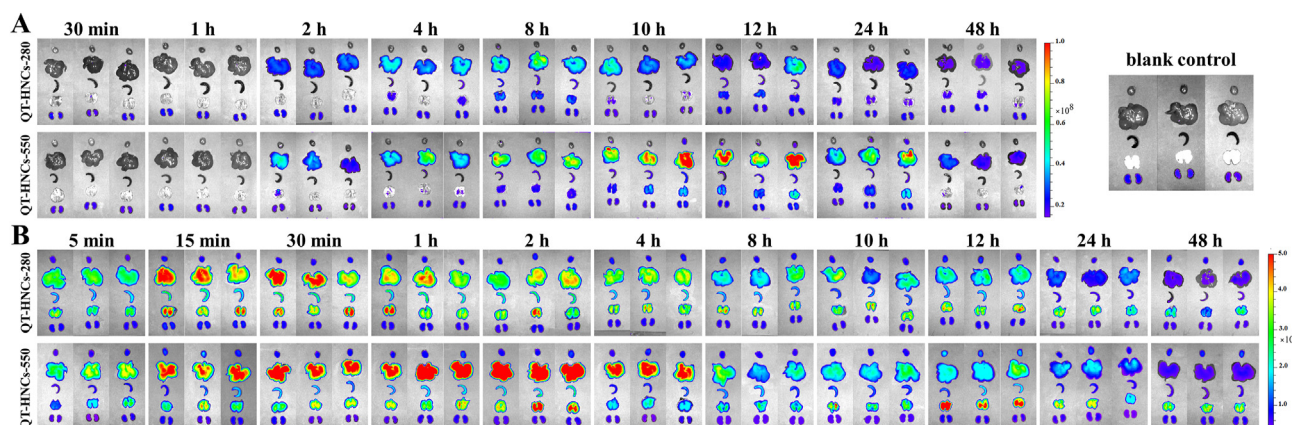


**Figure 4** *Ex vivo* imaging of major organs following oral (A) and intravenous (B) administration of QT-HNCs-280 and QT-HNCs-550, respectively. The rats treated without of QT-HNCs were used as blank control. From top to bottom in each panel: heart, liver, spleen, lung, kidney and brain.

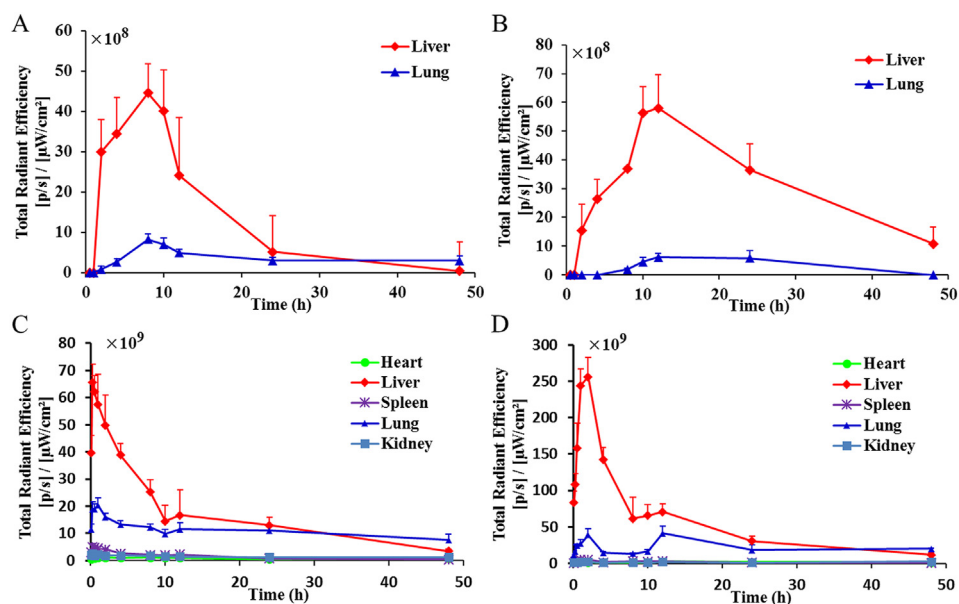


**Figure 5** Fluorescence quantification of major organs based on TRE following oral (A and B) and intravenous (C and D) administration of QT-HNCs-280 (A and C) and QT-HNCs-550 (B and D), respectively. Data are expressed as the mean  $\pm$  SD ( $n = 3$ ).

50.32 h $\cdot$  $\mu$ g/mL and 2.05  $\mu$ g/mL for QT-HNCs-550, respectively, indicating that a higher oral bioavailability of QT-HNCs-280. The faster dissolution and absorption of nanocrystals with smaller particle size may be responsible for the higher oral bioavailability of QT-HNCs-280<sup>55,56,58</sup>. However, there exists no significant difference in mean plasma QT concentrations at all-time points and pharmacokinetic parameters such as  $AUC_{0-t}$  and  $C_{max}$  of QT following intravenous administration of QT-HNCs (Fig. 6B and Table 3), which is similar to the results obtained from pharmacokinetics of integral QT-HNCs.

The QT concentration *versus* time curves of different organs following oral and intravenous administration of QT-HNCs are shown in Fig. 7. Their  $AUC_{0-t}$  was calculated from the QT concentration *versus* time curves by Pharmacokinetic software DAS 2.0 using statistical moment model (Table 4). After oral administration of QT-HNCs, the QT is mainly distributed in liver, lung and kidney, with the maximum distribution in the liver (Fig. 7A and B). No QT can be determined in heart and spleen, because the QT taken by heart and spleen is below the detection limit of HPLC. QT-HNCs-280 shows higher QT distribution in liver, lung and kidney than that of QT-HNCs-550 (Table 4), which can be explained by the fact that the higher oral bioavailability of QT-HNCs-280 results in its higher distribution in liver, lung and kidney.

Following intravenous administration of QT-HNCs, the QT is distributed in all tested organs, with the maximum distribution in

liver and the minimum distribution in heart (Fig. 7C and D, Table 4), confirming the higher accumulation of QT in RES organs and highlighting liver as the main destination for QT-HNCs. The QT-HNCs-550 shows higher accumulation of QT in liver and kidney as compared to QT-HNCs-280, which is consistent with the results of fluorescence quantification. The same reasons that larger nanocrystals dissolve slower and are easier recognized by RES might explain the higher accumulation of QT-HNCs-550<sup>42,55,56</sup>. However, compared with QT-HNCs-280, a lower accumulation of QT in lung, spleen and heart was found following intravenous administration of QT-HNCs-550, which is different from the result of fluorescence quantification. This may be due to that the observed fluorescence only reflects the undissolved or partially dissolved QT-HNCs but not free QT molecules<sup>40</sup>, whereas the detected QT in different organs include integral QT-HNCs and free QT molecules, the free QT molecules may account for major contribution for some organs.

### 3.6. Contribution analysis

Due to the fact that no fluorescent signal was observed in blood but obvious fluorescence in liver following oral administration of QT-HNCs, the absolute exposure of integral QT-HNCs was calculated based on the fluorescence intensity in liver to evaluate the contribution of integral QT-HNCs to oral bioavailability enhancement of QT. The absolute exposure of integral QT-HNCs

**Table 2** The  $AUC_{0-t}$ <sup>a</sup> of fluorescence distribution based on TRE in organs following oral and intravenous administration of QT-HNCs.

Organ	Oral ( $\times 10^{10}$ )		Intravenous ( $\times 10^{10}$ )	
	QT-HNCs-280	QT-HNCs-550	QT-HNCs-280	QT-HNCs-550
Heart	—	—	4.02 $\pm$ 0.17	7.58 $\pm$ 0.45 <sup>b</sup>
Liver	6.82 $\pm$ 1.12	15.27 $\pm$ 1.58 <sup>b</sup>	77.66 $\pm$ 6.05	259.63 $\pm$ 13.57 <sup>b</sup>
Spleen	—	—	6.60 $\pm$ 0.22	8.62 $\pm$ 0.34 <sup>b</sup>
Lung	1.73 $\pm$ 0.27	—	51.94 $\pm$ 5.70	107.16 $\pm$ 15.27 <sup>b</sup>
Kidney	—	—	6.84 $\pm$ 0.12	7.79 $\pm$ 1.78

<sup>a</sup>Unit: h $\cdot$ [p/s]/[ $\mu$ W/cm<sup>2</sup>]; —, not applicable. Data are presented as mean  $\pm$  SD ( $n = 3$ ).

<sup>b</sup> $P < 0.01$  vs. QT-HNCs-280.

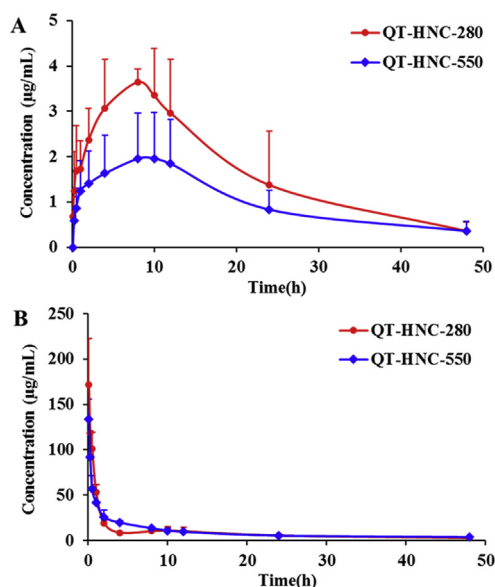


**Figure 6** Mean plasma concentration–time curves of quercetin following oral (A) and intravenous (B) administration of QT-HNCs-280 and QT-HNCs-550, respectively. Data are expressed as the mean  $\pm$  SD ( $n = 3$ ).

in liver based on TRE (Table 2) for QT-HNCs-280 and QT-HNCs-550 are as follows:

$$\text{QT-HNCs-280 : } F_{\text{abs}_{\text{NCS}}}(\%) = 6.82/77.66 \times 100 = 8.78\%$$

$$\text{QT-HNCs-550 : } F_{\text{abs}_{\text{NCS}}}(\%) = 15.27/259.63 \times 100 = 5.88\%$$

While the absolute exposure of integral QT-HNCs in liver based on ARE (Table S1) for QT-HNCs-280 and QT-HNCs-550 are 8.15% and 5.68%, respectively. The TRE can roughly represent the total amount of nanocrystals, whereas ARE stands for the concentration of nanocrystals in tested organs. The results obtained from the TRE and ARE show similar absolute exposure of integral QT-HNCs in liver. They can confirm each other to ensure the reliability of the results.

The absolute exposure of total QT in liver for QT-HNCs-280 and QT-HNCs-550 are as follows:

$$\text{QT-HNCs-280 : } F_{\text{abs}_{\text{QT}}}(\%) = 146.90/673.82 \times 100 = 21.80\%$$

$$\text{QT-HNCs-550 : } F_{\text{abs}_{\text{QT}}}(\%) = 117.91/1015.80 \times 100 = 11.61\%$$

While the absolute bioavailability of QT following oral administration of QT-HNCs are 18.50% for QT-HNCs-280 and 10.76% for QT-HNCs-550, which are similar to the absolute exposure of total QT in liver (21.80% for QT-HNCs-280 and 11.61% for QT-HNCs-550). In some extent, these results suggested that the absolute exposure of integral QT-HNCs and total QT in the liver could be used to estimate the contribution of integral QT-HNCs to oral bioavailability enhancement of QT.

The contribution of absorption of integral QT-HNCs to oral bioavailability enhancement of QT based on TRE are as follows:

$$\text{QT-HNCs-280 : } \text{Contribution}(\%) = 8.78/21.8 \times 100 = 40.27\%$$

$$\text{QT-HNCs-550 : } \text{Contribution}(\%) = 5.88/11.61 \times 100 = 50.65\%$$

While the contribution of absorption of integral QT-HNCs to oral bioavailability enhancement of QT based on ARE is 37.39% for QT-HNCs-280 and 48.89% for QT-HNCs-550, respectively. It is worth noting that the contribution of absorption of integral QT-HNCs to oral bioavailability enhancement of QT is surprisingly high. However, only about 3% integral QT-HNCs was absorbed according to the rough estimation from the TRE values in small intestine and liver in our previous study<sup>40</sup>. According to this result (about 3% integral QT-HNCs absorbed), the contribution of absorption of integral QT-HNCs to oral bioavailability enhancement of QT is 13.76% for QT-HNCs-280 and 25.84% for QT-HNCs-550.

A significant higher contribution of absorption of integral QT-HNCs to oral bioavailability enhancement of QT was obtained in this study as compared to our previous study. The re-illumination of the fluorescence in hepatic tissues may results in higher absolute exposure of integral QT-HNCs in liver, leading to higher contribution of absorption of integral QT-HNCs to oral bioavailability enhancement of QT. In fact, if the re-illumination of the fluorescence in hepatic tissues brings about interference, there may be more interference in liver for intravenous administration of QT-HNCs due to more P2 probes entering the body, which may lead to lower absolute exposure of integral QT-HNCs and thereby causing lower but not higher contribution of absorption of integral QT-HNCs. Therefore, we believe more that the surprisingly high contribution of absorption of integral QT-HNCs may be attributed to the imprecise semi-quantification method of fluorescence intensity. More imprecise quantitative methods are needed to accurately quantify the intact nanocrystals *in vivo*, ensuring the

**Table 3** Main pharmacokinetic parameters of QT following oral and intravenous administration of QT-HNCs.

Parameter	Oral		Intravenous	
	QT-HNCs-280	QT-HNCs-550	QT-HNCs-280	QT-HNCs-550
AUC <sub>0-t</sub> (h·µg/mL)	82.40 $\pm$ 12.22	50.32 $\pm$ 5.88 <sup>a</sup>	445.49 $\pm$ 58.02	467.67 $\pm$ 59.96
MRT <sub>0-t</sub> (h)	14.50 $\pm$ 1.97	16.51 $\pm$ 1.63	12.45 $\pm$ 1.09	13.42 $\pm$ 0.63
<i>t</i> <sub>1/2z</sub> (h)	11.31 $\pm$ 1.52	14.65 $\pm$ 5.01	18.18 $\pm$ 3.57	21.84 $\pm$ 9.16
<i>T</i> <sub>max</sub> (h)	8.67 $\pm$ 1.15	10 $\pm$ 2	—	—
<i>C</i> <sub>max</sub> (µg/mL)	3.70 $\pm$ 0.28	2.05 $\pm$ 0.26 <sup>b</sup>	171.84 $\pm$ 50.51	134.17 $\pm$ 21.46

—, Not applicable. Data are presented as mean  $\pm$  SD ( $n = 3$ ).

<sup>a</sup> $P < 0.05$ .

<sup>b</sup> $P < 0.01$  vs. QT-HNCs-280.

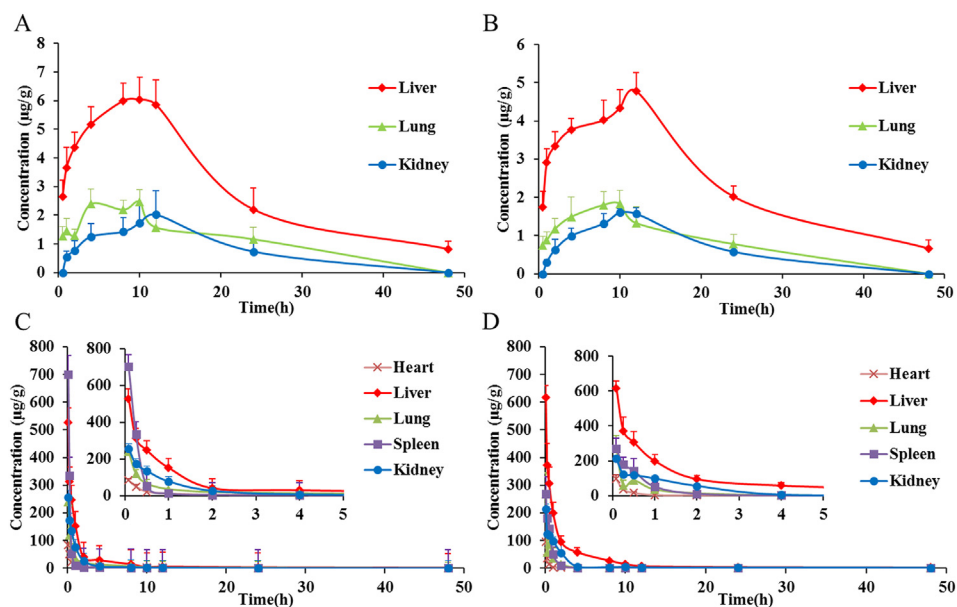


**Figure 7** Mean quercetin concentration–time curves in major organs following oral (A and B) and intravenous (C and D) administration of QT-HNCs-280 (A and C) and QT-HNCs-550 (B and D), respectively. Data are expressed as the mean  $\pm$  SD ( $n = 3$ ).

**Table 4** The  $AUC_{0-t}$ <sup>a</sup> of quercetin distribution in organs following oral and intravenous administration of QT-HNCs.

Organ	Oral		Intravenous	
	QT-HNCs-280	QT-HNCs-550	QT-HNCs-280	QT-HNCs-550
Heart	—	—	89.16 $\pm$ 18.94	42.17 $\pm$ 6.51 <sup>c</sup>
Liver	146.90 $\pm$ 20.28	117.91 $\pm$ 5.89 <sup>b</sup>	673.82 $\pm$ 37.85	1015.80 $\pm$ 150.14 <sup>c</sup>
Spleen	—	—	251.15 $\pm$ 29.07	207.68 $\pm$ 43.34
Lung	40.75 $\pm$ 4.57	30.33 $\pm$ 5.37 <sup>b</sup>	241.44 $\pm$ 26.84	174.57 $\pm$ 29.90 <sup>b</sup>
Kidney	39.14 $\pm$ 4.42	25.86 $\pm$ 2.83 <sup>c</sup>	271.33 $\pm$ 26.95	375.45 $\pm$ 85.36

<sup>a</sup>Unit:  $h \cdot \mu\text{g}/\text{mL}$ ; —, not applicable. Data are presented as mean  $\pm$  SD ( $n = 3$ ).

<sup>b</sup> $P < 0.05$ .

<sup>c</sup> $P < 0.01$  vs. QT-HNCs-280.

precise calculation of the contribution of the absorption of intact QT-HNCs to the overall bioavailability enhancement.

#### 4. Conclusions

In this study, the biological fate of QT-HNCs with particle sizes around 280 nm (QT-HNCs-280) and 550 nm (QT-HNCs-550) following oral and intravenous administration was explored by self-discriminating hybrid nanocrystals technique and HPLC method. Live imaging and *ex vivo* imaging demonstrated that QT-HNCs could reside *in vivo* as intact nanocrystals for as long as 48 h following oral and intravenous administration. A higher accumulation of integral QT-HNCs in liver and lung was observed for both oral and intravenous administration of QT-HNCs. The particle size affects the absorption and distribution of integral QT-HNCs and total QT following oral and intravenous administration of QT-HNCs. As compared to QT-HNCs-550, QT-HNCs-280 with smaller particle size is more easily absorbed, but dissolves faster *in vivo*, leading to higher distribution of QT (146.90 vs. 117.91  $h \cdot \mu\text{g}/\text{mL}$ ) but lower accumulation of integral nanocrystals ( $6.8 \cdot 10^{10}$  vs.  $15.27 \cdot 10^{10}$   $h \cdot [p/s]/[\mu\text{W}/\text{cm}^2]$ ) in liver following oral administration. Due to its slower dissolution and enhanced recognition by RES, QT-HNCs-550 with larger diameter shows higher liver distribution for both of QT (1015.80  $h \cdot \mu\text{g}/\text{mL}$ ) and integral nanocrystals ( $259.63 \cdot 10^{10}$   $h \cdot [p/s]/[\mu\text{W}/\text{cm}^2]$ ) than those of QT-HNCs-280 (673.82  $h \cdot \mu\text{g}/\text{mL}$  &  $77.66 \cdot 10^{10}$   $h \cdot [p/s]/[\mu\text{W}/\text{cm}^2]$ ) following intravenous administration. However, in spite of higher accumulation of integral nanocrystals, QT-HNCs-550 shows lower QT distribution in heart, spleen and lung than those of QT-HNCs-280 following intravenous administration. Moreover, the absolute exposure of integral QT-HNCs and total QT were calculated based on fluorescence intensity and QT concentrations in liver to estimate the contribution of absorption of integral QT-HNCs to oral bioavailability enhancement of QT. The absolute exposure of integral QT-HNCs in liver following oral administration of QT-HNCs are 8.78% for QT-HNCs-280 and 5.88% for QT-HNCs-550, while the absolute exposure of total QT for QT-HNCs-280 and QT-HNCs-550 are 21.80% and 11.61%, respectively. Owing to imprecise quantification method, a surprisingly high contribution of integral QT-HNCs to oral bioavailability enhancement of QT (40.27% for QT-HNCs-280 and 50.65% for QT-HNCs-550) was obtained by

precise calculation of the contribution of the absorption of intact QT-HNCs to the overall bioavailability enhancement. Due to its slower dissolution and enhanced recognition by RES, QT-HNCs-550 with larger diameter shows higher liver distribution for both of QT (1015.80  $h \cdot \mu\text{g}/\text{mL}$ ) and integral nanocrystals ( $259.63 \cdot 10^{10}$   $h \cdot [p/s]/[\mu\text{W}/\text{cm}^2]$ ) than those of QT-HNCs-280 (673.82  $h \cdot \mu\text{g}/\text{mL}$  &  $77.66 \cdot 10^{10}$   $h \cdot [p/s]/[\mu\text{W}/\text{cm}^2]$ ) following intravenous administration. However, in spite of higher accumulation of integral nanocrystals, QT-HNCs-550 shows lower QT distribution in heart, spleen and lung than those of QT-HNCs-280 following intravenous administration. Moreover, the absolute exposure of integral QT-HNCs and total QT were calculated based on fluorescence intensity and QT concentrations in liver to estimate the contribution of absorption of integral QT-HNCs to oral bioavailability enhancement of QT. The absolute exposure of integral QT-HNCs in liver following oral administration of QT-HNCs are 8.78% for QT-HNCs-280 and 5.88% for QT-HNCs-550, while the absolute exposure of total QT for QT-HNCs-280 and QT-HNCs-550 are 21.80% and 11.61%, respectively. Owing to imprecise quantification method, a surprisingly high contribution of integral QT-HNCs to oral bioavailability enhancement of QT (40.27% for QT-HNCs-280 and 50.65% for QT-HNCs-550) was obtained by

comparing the absolute exposure of integral QT-HNCs and total QT in liver. In summary, the present study revealed significant difference in absorption and biodistribution between integral nanocrystals and overall drugs following oral and intravenous administration of QT-HNCs. Although not accurate enough, it provided a meaningful reference for the contribution of integral nanocrystals to overall bioavailability enhancement.

### Acknowledgments

This work was supported by the National Natural Science Foundation of China (Nos. 81803741 and 81873092).

### Author contributions

Hailong Yuan and Weifeng Zhu designed the research. Baode Shen and Chengying Shen carried out the experiments and performed data analysis. Hailong Yuan provided experimental drugs and quality control. Baode Shen wrote the manuscript. Baode Shen and Hailong Yuan revised the manuscript. All of the authors have read and approved the final manuscript.

### Conflicts of interest

The authors have no conflicts of interest to declare.

### Appendix A. Supporting information

Supporting data to this article can be found online at <https://doi.org/10.1016/j.apsb.2021.02.015>.

### References

- Ren XT, Qi JP, Wu W, Yin ZN, Li TL, Lu Y. Development of carrier-free nanocrystals of poorly water-soluble drugs by exploring metastable zone of nucleation. *Acta Pharm Sin B* 2019;**9**:118–27.
- Mohammad IS, Hu HY, Yin LF, He W. Drug nanocrystals: fabrication methods and promising therapeutic applications. *Int J Pharm* 2019;**562**:187–202.
- Gujar K, Wairkar S. Nanocrystal technology for improving therapeutic efficacy of flavonoids. *Phytomedicine* 2020;**71**:153240.
- Lai F, Schlich M, Pireddu R, Fadda AM, Sinico C. Nanocrystals as effective delivery systems of poorly water-soluble natural molecules. *Curr Med Chem* 2019;**26**:4657–80.
- Shen BD, Wu N, Shen CY, Zhang FC, Wu Y, Xu PH, et al. Hyperoside nanocrystals for HBV treatment: process optimization, *in vitro* and *in vivo* evaluation. *Drug Dev Ind Pharm* 2016;**42**:1772–81.
- Lu Y, Chen Y, Gemeinhart RA, Wu W, Li T. Developing nanocrystals for cancer treatment. *Nanomedicine* 2015;**10**:2537–52.
- Müller RH, Gohla S, Keck CM. State of the art of nanocrystals—special features, production, nanotoxicology aspects and intracellular delivery. *Eur J Pharm Biopharm* 2011;**78**:1–9.
- Fontana F, Figueiredo P, Zhang P, Hirvonen JT, Liu DF, Santos HA. Production of pure drug nanocrystals and nano co-crystals by confinement methods. *Adv Drug Deliv Rev* 2018;**131**:3–21.
- Chen ZJ, Wu W, Lu Y. What is the future for nanocrystal-based drug-delivery systems?. *Ther Deliv* 2020;**11**:225–9.
- Wu W, Lu Y, Qi JP. Editorial: persistent endeavors for the enhancement of dissolution and oral bioavailability. *Acta Pharm Sin B* 2019;**9**:2–3.
- Rabinow BE. Nanosuspensions in drug delivery. *Nat Rev Drug Discov* 2004;**3**:785–96.
- Müller RH, Keck CM. Twenty years of drug nanocrystals: where are we, and where do we go?. *Eur J Pharm Biopharm* 2012;**80**:1–3.
- Gao L, Liu GY, Ma JL, Wang XQ, Zhou L, Li X, et al. Application of drug nanocrystal technologies on oral drug delivery of poorly soluble drugs. *Pharm Res* 2013;**30**:307–24.
- Jacob S, Nair AB, Shah J. Emerging role of nanosuspensions in drug delivery systems. *Biomater Res* 2020;**24**:3.
- Patel V, Sharma OP, Mehta T. Nanocrystal: a novel approach to overcome skin barriers for improved topical drug delivery. *Expert Opin Drug Deliv* 2018;**15**:351–68.
- Lu Y, Li Y, Wu W. Injected nanocrystals for targeted drug delivery. *Acta Pharm Sin B* 2016;**6**:106–13.
- Liu T, Yu XX, Yin HP, Möschwitzer JP. Advanced modification of drug nanocrystals by using novel fabrication and downstream approaches for tailor-made drug delivery. *Drug Deliv* 2019;**26**:1092–103.
- Shi TT, Lv YJ, Huang WZ, Fang ZZ, Qi JP, Chen ZJ, et al. Enhanced transdermal delivery of curcumin nanosuspensions: a mechanistic study based on co-localization of particle and drug signals. *Int J Pharm* 2020;**588**:119737.
- Pardhi VP, Verma T, Flora SJS, Chandasana H, Shukla R. Nanocrystals: an overview of fabrication, characterization and therapeutic applications in drug delivery. *Curr Pharmaceut Des* 2018;**24**:5129–46.
- Cheng ZY, Lian YM, Kamal Z, Ma X, Chen JJ, Zhou XB, et al. Nanocrystals technology for pharmaceutical science. *Curr Pharmaceut Des* 2018;**24**:2497–507.
- Malamatari M, Somavarapu S, Taylor KM, Buckton G. Solidification of nanosuspensions for the production of solid oral dosage forms and inhalable dry powders. *Expert Opin Drug Deliv* 2016;**13**:435–50.
- Wang YC, Zheng Y, Zhang L, Wang QW, Zhang DR. Stability of nanosuspensions in drug delivery. *J Control Release* 2013;**172**:1126–41.
- Gao L, Liu GY, Ma JL, Wang XQ, Zhou L, Li X. Drug nanocrystals: *In vivo* performances. *J Control Release* 2012;**160**:418–30.
- Shah DA, Murdande SB, Dave RH. A Review: Pharmaceutical and pharmacokinetic aspect of nanocrystalline suspensions. *J Pharmacol Sci* 2016;**105**:10–24.
- Lu Y, Qi JP, Dong XC, Zhao WL, Wu W. The *in vivo* fate of nanocrystals. *Drug Discov Today* 2017;**22**:744–50.
- Wu W, Li TL. Unraveling the *in vivo* fate and cellular pharmacokinetics of drug nanocarriers. *Adv Drug Deliv Rev* 2019;**143**:1–2.
- Miao XQ, Li Y, Wang XQ, Lee SM, Zheng Y. Transport mechanism of coumarin 6 nanocrystals with two particle sizes in MDCKII monolayer and larval zebrafish. *ACS Appl Mater Interfaces* 2016;**8**:12620–30.
- Vidlářová L, Romero GB, Hanuš J, Štěpánek F, Müller RH. Nanocrystals for dermal penetration enhancement—effect of concentration and underlying mechanisms using curcumin as model. *Eur J Pharm Biopharm* 2016;**104**:216–25.
- Chan CPY, Bruemmel Y, Seydack M, Sin KK, Wong LW, Merisko-Liversidge E, et al. Nanocrystal biolabels with releasable fluorophores for immunoassays. *Anal Chem* 2004;**76**:3638–45.
- Corrias F, Schlich M, Sinico C, Pireddu R, Valenti D, Fadda AM, et al. Nile red nanosuspensions as investigative model to study the follicular targeting of drug nanocrystals. *Int J Pharm* 2017;**524**:1–8.
- Zhao RS, Hollis CP, Zhang H, Sun LL, Gemeinhart RA, Li TL. Hybrid nanocrystals: achieving concurrent therapeutic and bioimaging functionalities toward solid tumors. *Mol Pharm* 2011;**8**:1985–91.
- Hollis CP, Weiss HL, Leggas M, Evers BM, Gemeinhart RA, Li TL. Biodistribution and bioimaging studies of hybrid paclitaxel nanocrystals: lessons learned of the EPR effect and image-guided drug delivery. *J Control Release* 2013;**172**:12–21.
- Hollis CP, Weiss HL, Evers BM, Gemeinhart RA, Li TL. *In vivo* investigation of hybrid Paclitaxel nanocrystals with dual fluorescent probes for cancer theranostics. *Pharm Res* 2014;**31**:1450–9.

34. Chen Y, Li TL. Cellular Uptake Mechanism of paclitaxel nanocrystals determined by confocal imaging and kinetic measurement. *AAPS J* 2015;**17**:1126–34.
35. Gao W, Chen Y, Thompson DH, Park K, Li TL. Impact of surfactant treatment of paclitaxel nanocrystals on biodistribution and tumor accumulation in tumor-bearing mice. *J Control Release* 2016;**237**:168–76.
36. Yang YQ, Lv YJ, Shen CY, Shi TT, Wu W. *In vivo* dissolution of poorly water-soluble drugs: proof of concept based on fluorescence bioimaging. *Acta Pharm Sin B* 2020. Available from: <https://doi.org/10.1016/j.apsb.2020.08.002>.
37. Zhang JF, Corpstein CD, Li TL. Intracellular uptake of nanocrystals: probing with aggregation-induced emission of fluorescence and kinetic modeling. *Acta Pharm Sin B* 2020. Available from: <https://doi.org/10.1016/j.apsb.2020.09.017>.
38. Hu XW, Dong XC, Lu Y, Qi JP, Zhao WL, Wu W. Bioimaging of nanoparticles: The crucial role of discriminating nanoparticles from free probes. *Drug Discov Today* 2017;**22**:382–7.
39. Gao W, Lee D, Meng ZJ, Li TL. Exploring intracellular fate of drug nanocrystals with crystal-integrated and environment-sensitive fluorophores. *J Control Release* 2017;**267**:214–22.
40. Shen CY, Yang YQ, Shen BD, Xie YK, Qi JP, Dong XC, et al. Self-discriminating fluorescent hybrid nanocrystals: efficient and accurate tracking of translocation *via* oral delivery. *Nanoscale* 2017;**10**:436–50.
41. Xie YK, Shi BK, Xia F, Qi JP, Dong XC, Zhao WL, et al. Epithelia transmembrane transport of orally administered ultrafine drug particles evidenced by environment sensitive fluorophores in cellular and animal studies. *J Control Release* 2018;**270**:65–75.
42. Wang T, Qi JP, Ding N, Dong XC, Zhao WL, Lu Y, et al. Tracking translocation of self-discriminating curcumin hybrid nanocrystals following intravenous delivery. *Int J Pharm* 2018;**546**:10–9.
43. Lu Y, Lv YJ, Li TL. Hybrid drug nanocrystals. *Adv Drug Deliv Rev* 2019;**143**:115–33.
44. Wang YF, Zhang YX, Wang JJ, Liang XJ. Aggregation-induced emission (AIE) fluorophores as imaging tools to trace the biological fate of nano-based drug delivery systems. *Adv Drug Deliv Rev* 2019;**143**:161–76.
45. Qi JP, Hu XW, Dong XC, Lu Y, Lu HP, Zhao WL, et al. Towards more accurate bioimaging of drug nanocarriers: turning aggregation-caused quenching into a useful tool. *Adv Drug Deliv Rev* 2019;**143**:206–25.
46. Chen TK, He B, Tao JS, He Y, Deng HL, Wang XQ, et al. Application of Förster Resonance Energy Transfer (FRET) technique to elucidate intracellular and *in vivo* biofate of nanomedicines. *Adv Drug Deliv Rev* 2019;**143**:177–205.
47. He HS, Wang LT, Ma YH, Yang YQ, Lv YJ, Zhang ZC, et al. The biological fate of orally administered mPEG-PDLLA polymeric micelles. *J Control Release* 2020;**327**:725–36.
48. Yu Z, Fan WF, Wang LT, He HS, Lv YJ, Qi JP, et al. Slowing down lipolysis significantly enhances the oral absorption of intact solid lipid nanoparticles. *Biomater Sci* 2019;**7**:4273–82.
49. He HS, Zhang J, Xie YC, Lu Y, Qi JP, Ahmad E, et al. Bioimaging of intravenous polymeric micelles based on discrimination of integral particles using an environment-responsive probe. *Mol Pharm* 2016;**13**:4013–9.
50. He HS, Jiang SF, Xie YC, Lu Y, Qi JP, Dong XC, et al. Reassessment of long circulation *via* monitoring of integral polymeric nanoparticles justifies a more accurate understanding. *Nanoscale Horiz* 2018;**3**:397–407.
51. Xia F, Fan WF, Jiang SF, Ma YH, Lu Y, Qi JP, et al. Size-dependent translocation of nanoemulsions *via* oral delivery. *ACS Appl Mater Interfaces* 2017;**9**:21660–72.
52. Hu XW, Fan WF, Yu Z, Lu Y, Qi JP, Zhang J, et al. Evidence does not support absorption of intact solid lipid nanoparticles *via* oral delivery. *Nanoscale* 2016;**8**:7024–35.
53. Hu XW, Zhang J, Yu Z, Xie YC, He HS, Qi JP, et al. Environment-responsive aza-BODIPY dyes quenching in water as potential probes to visualize the *in vivo* fate of lipid-based nanocarriers. *Nanomedicine* 2015;**11**:1939–48.
54. Gotch F, Nadell J, Edelman IS. Gastrointestinal water and electrolytes. IV. The equilibration of deuterium oxide (D<sub>2</sub>O) in gastrointestinal contents and the proportion of total body water (T.B.W.) in the gastrointestinal tract. *J Clin Invest* 1957;**36**:289–96.
55. Bi C, Miao XQ, Chow SF, Wu WJ, Yan R, Liao YH, et al. Particle size effect of curcumin nanosuspensions on cytotoxicity, cellular internalization, *in vivo* pharmacokinetics and biodistribution. *Nanomedicine* 2017;**13**:943–53.
56. Wang XH, Liu Y, Shen CY, Shen BD, Zhong RN, Yuan HL. Effect of particle size on *in vitro* and *in vivo* behavior of astilbin nanosuspensions. *J Drug Deliv Sci Technol* 2019;**52**:778–83.
57. Zhang WL, Wang GJ, See E, Shaw JP, Baguley BC, Liu JP, et al. Post-insertion of poloxamer 188 strengthened liposomal membrane and reduced drug irritancy and *in vivo* precipitation, superior to PEGylation. *J Control Release* 2015;**203**:161–9.
58. Yao MF, He LL, McClements DJ, Xiao H. Uptake of gold nanoparticles by intestinal epithelial cells: impact of particle size on their absorption, accumulation, and toxicity. *J Agric Food Chem* 2015;**63**:8044–9.
59. Sigfridsson K, Skantze P, Skantze U, Svensson L, Lofgren L, Nordell P, et al. Nanocrystal formulations of a poorly soluble drug. 2. Evaluation of nanocrystal liver uptake and distribution after intravenous administration to mice. *Int J Pharm* 2017;**524**:248–56.
60. Li HL, Zhao XB, Ma YK, Zhai GX, Li LB, Lou HX. Enhancement of gastrointestinal absorption of quercetin by solid lipid nanoparticles. *J Control Release* 2009;**133**:238–44.